SERBIAN JOURNAL OF ELECTRICAL ENGINEERING
Vol. 11, No. 2, June 2014, 315-337

UDC: 621.382:621.314.1 **DOI: 10.2298/SJEE1402315M**

Multiple Low Frequency Dual Reference PWM Control of a Grid Connected Photovoltaic Three Phase NPC Inverter with DC/DC Boost Converter

Rabiaa Mechouma[1], Boubekeur Azoui[1]

Abstract: In recent years, power demand of industrial applications has increased significantly reaching some megawatts. The use of multilevel converters for applications of medium and high powers is proposed as a solution to drawback semiconductor technology. A multilevel converter not only achieves high power ratings, but also enables the use of renewable energy sources. Renewable energy sources such as photovoltaic can be easily interfaced to a multilevel converter system for a high power application. This paper presents the simulation study in Matlab/Simulink of a grid connected photovoltaic three phase Neutral Point Clamped (NPC) inverter with DC/DC boost converter for constant and variable solar radiation.

Keywords: Grid-connected PV systems, Multi level inverter, Multiple low frequency PWM, LCL filter, MPPT controller.

1 Introduction

Renewable energy sources such as photovoltaic, wind, and fuel cells can be easily interfaced to a multilevel converter system for a high power application [1 – 4]. The concept of multilevel converters has been introduced since 1975 [5]. Capacitors, batteries, and renewable energy voltage sources can be used as multiple dc voltage sources. The commutation of the power switches aggregate these multiple dc sources in order to achieve high voltage at the output; however, the rated voltage of the power semiconductor switches depends only on the rating of the dc voltage sources to which they are connected. Among these converters, the three phase three levels NPC inverters used in photovoltaic systems connected to the grid are mentioned. The simulation study in Matlab/Simulink of a grid connected photovoltaic three phase NPC inverter with DC/DC boost converter has been presented in this paper. A photovoltaic generator of N_p solar modules branches in parallel ($N_P = 10$) containing N_S modules in series ($N_S = 19$) is used. Each parallel branch is connected to an inverter via a DC/DC boost converter. This converter is controlled by a current generated by a controller based on a maximum power point tracking (MPPT)

[1]LEB, Department of Electrical Engineering, University of Batna, 05000, Algeria, E-mail: mechou_ra@yahoo.fr

algorithm known as the Perturbation and Observation (P&O). The inverter control is based on a multiple low frequency dual reference PWM strategy accompanied by a PID controller. The study has been done for a constant and a variable solar radiation and the obtained results are discussed.

2 Grid Connected Photovoltaic System Structure

The global system, shown in Fig. 1, consists of a Photovoltaic generator (PVG), two identical input capacitors *C* and *C'* to form a capacitive divider, an inverter composed of 12 switches with six diodes connected to the neutral point, an output filter (LCL) and a DC/DC boost converter. The whole system is connected to the grid.

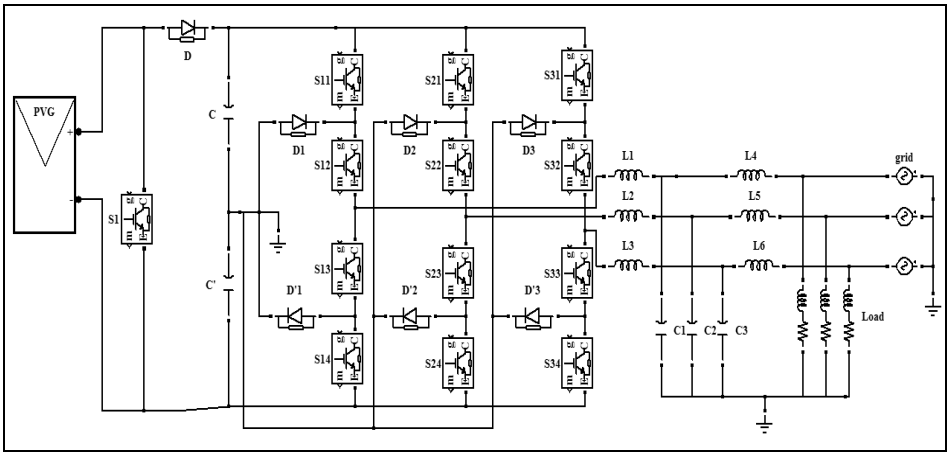

Fig. 1 – *Photovoltaic global grid connected system.*

2.1 PVG System model

Many models are developed to represent photovoltaic generator (PVG) *I-V* characteristic [6]. In this work the one diode model, whose diagram is shown in Fig. 2, is chosen. The output current *I* of solar cell is given by (1)

$$I = I_L - I_D \,, \tag{1}$$

where I_L is the photocurrent and I_D is the diode current. The photocurrent I_L varies with the irradiance and temperature, it is determined with respect to the values given in the standard test conditions (STC):

$$I_L = \left(\frac{G}{G_{ref}} \right) I_{SC\_ref} \left[1 + K_0 \left(T - T_{ref} \right) \right], \tag{2}$$

where: G_{ref} is the reference value of the irradiation (G_{ref} = 1000 W/m^2), T_{ref} the reference value of the temperature (T_{ref} = 25°C) and I_{sc_ref} the short circuit current at the STC.

T and *G* are respectively temperature and irradiating operation of the cell.

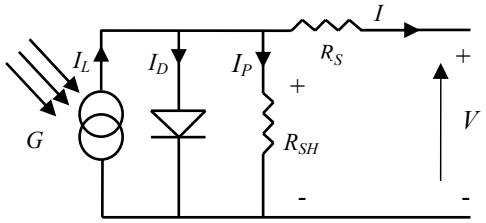

Fig. 2 – *One diode circuit of the PV model.*

K_0 is the temperature coefficient of the current which is given by the following equation:

$$\mathrm{r}\,K_0 = \frac{I_{SC\_T} - I_{SC\_T_{ref}}}{T - T_{ref}}, \tag{3}$$

where I_{SC_T} is the current of the PV cell at the operating temperature and $I_{SC\_T_{ref}}$ the current of the PV cell at the reference temperature T_{ref}.

The diode current is given by:

$$I_D = I_0\left[\left(\exp\left(q\frac{V + R_S I}{nkT}\right)\right) - 1\right], \tag{4}$$

where *k* is the Boltzmann's constant ($k = 1.38065\times10^{-23}$ J/K), *q* the electrical charge of the electron with a value equal to 1.60217733×10^{-19} C, n is the quality factor which varies typically from 1 to 2, R_S is the series resistance of the PV module and I_0.

The reverse bias saturation current which varies with temperature "*T*" according to the following expression:

$$I_0 = I_{0\_T_{ref}}\left(\frac{T}{T_{ref}}\right)^{\frac{3}{n}} \exp\left(\frac{-qV_g}{nk}\left(\frac{1}{T} - \frac{1}{T_{ref}}\right)\right), \tag{5}$$

where V_g is the Band gap voltage (for the Silicon V_g = 1.11 V) and $I_{0\_T_{ref}}$ the reverse bias saturation current at the reference temperature.

The saturation current of the diode is given by:

$$I_{0\_T_{ref}} = \frac{I_{SC\_T_{ref}}}{\left(\exp\left(\frac{qV_{OC\_T_{ref}}}{nkT_{ref}}\right)-1\right)}, \tag{6}$$

where V_{oc} is the open-circuit voltage of the PV cell, $I_{SC\_T_{ref}}$ and $V_{OC\_T_{ref}}$ are respectively the short circuit current and the open circuit voltage at the STC. A series resistance R_S was included:

$$R_S = \left(-\frac{\mathrm{d}V}{\mathrm{d}I}\right)_{V_{OC}} - \frac{1}{X_V}, \tag{7}$$

where:

$$X_V = I_{0\_T_{ref}} \frac{q}{nkT_{ref}} \exp\left(q\frac{V_{OC\_T_{ref}}}{nkT_{ref}}\right). \tag{8}$$

The shunt resistance R_{SH} is neglected.

The overall equation for modeling the cell is:

$$I = I_L - I_0\left[\exp\left(q\frac{V+R_SI}{nkT}\right)-1\right], \tag{9}$$

where V and I are the output voltage and the output current of the cell. I_L is the photocurrent, q, n, k are already defined.

In this work a PVG, which consists of N_P branches of N_S PV modules in each branch, is used:

$$V_{PVG} = N_S \times V_{Panel}, \tag{10}$$

$$I_{PVG} = N_P \times I_{Panel}. \tag{11}$$

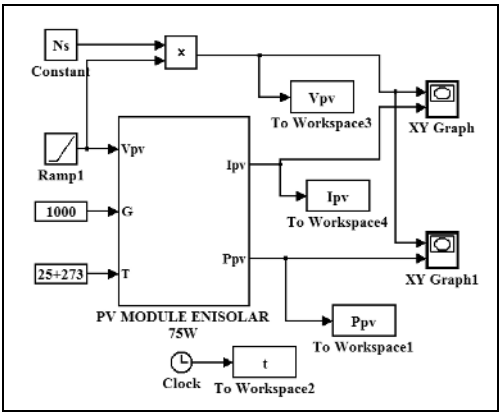

Fig. 3 – *Simulation of the PV module ENIESOLAR.*

2.2 DC/DC boost converter and its control

2.2.1 DC/DC boost converter model

The DC/DC boost converter model is given in Fig. 4.

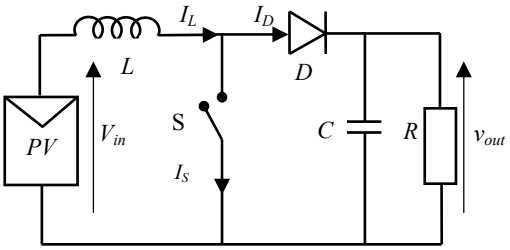

Fig. 4 – *Boost converter schematic.*

When the converter operates in continuous mode, the current through the inductor (I_L) never falls to zero. In the case of an ideal converter operating in steady conditions, the output voltage can be calculated as follows [7]:

During the On-state, the switch "S" is closed, which let the input voltage (V_{in}) appearing across the inductor and causes a change in current (I_L) flowing through the inductor during a time period (t) by the expression:

$$\frac{\Delta I_L}{\Delta t} = \frac{V_{in}}{L}. \tag{12}$$

At the end of the On-state, the increase of I_L is therefore:

$$\Delta I_{L_{on}} = \frac{1}{L}\int_0^{DT} V_{in}\,\mathrm{d}\,t = \frac{DT}{L}V_{in}, \tag{13}$$

where D is the duty cycle; it represents the fraction of the commutation period T during which the switch is on. Therefore D ranges between 0 and 1.

During the Off-state, the switch "S" is open, so the inductor current flows through the load. If a zero voltage drop in the diode and a capacitor large enough for its voltage to remain constant are considered, then the evolution of I_L is:

$$V_{in} - V_{out} = L\frac{\mathrm{d}\,I_L}{\mathrm{d}\,t}. \tag{14}$$

Therefore, the variation of I_L during the Off-period is:

$$DI_{L_{off}} = \int_{DT}^{T} \frac{\left(V_{in} - V_{out}\right)\mathrm{d}\,t}{L} = \frac{\left(V_{in} - V_{out}\right)\left(1-D\right)T}{L}. \tag{15}$$

As the converter operates in steady-state conditions, the amount of energy stored in each of its components has to be the same at the beginning and at the end of a commutation cycle. In particular, the energy stored in the inductor is given by:

$$E = \frac{1}{2} L I_L^2 . \tag{16}$$

At the start and the end of the commutation cycle, the inductor current has to be the same. This means the overall change in the current is zero:

$$\Delta I_{L_{on}} + \Delta I_{L_{off}} = 0 . \tag{17}$$

Substituting $\Delta I_{L_{on}}$ and $\Delta I_{L_{off}}$ by their expressions yields:

$$\Delta I_{L_{on}} + \Delta I_{L_{off}} = \frac{V_{in} DT}{L} + \frac{(V_{in} - V_{out})(1-D)T}{L} = 0. \tag{18}$$

This can be written as:

$$\frac{V_{out}}{V_{in}} = \frac{1}{1-D} . \tag{19}$$

In turn, this reveals the duty cycle to be:

$$D = 1 - \frac{V_{in}}{V_{out}} , \tag{20}$$

(where: $0 \le D \le 1$), it has:

$$V_{out} = \frac{1}{C} \int I_{out} \, \mathrm{d}t . \tag{21}$$

This after derivation becomes:

$$\frac{\mathrm{d}V_{out}}{\mathrm{d}t} = \frac{1}{C}\left(I_L - \frac{V_{out}}{R} \right) = \frac{1}{C}\left[I_L - \frac{1}{R}\left(\frac{V_{in}}{1-D} \right) \right], \tag{22}$$

where L, R and C are respectively the inductor, the resistor and the capacitor of the DC/DC converter, V_{in} and V_{out} are respectively the input voltage and the output voltage of the DC/DC converter.

The efficiency $\eta_{DC/DC}$ of the boost DC/DC converter is given by:

$$\eta_{DC/DC} = \frac{V_{out} \times I_{out}}{V_{in} \times I_L} = \frac{P_{out}}{P_{in}} . \tag{23}$$

2.2.2 MPPT control

The boost (step-up) DC/DC converter is modelled as a block where inputs are the voltage delivered by the PV array and the current generated by the MPPT controller. This MPPT is based on a search algorithm called perturb and observe (P&O) [8].

2.3 Model of the NPC inverter

As shown in Fig. 1 the NPC inverter is formed by three legs. Each leg has four IGBTs connected in series and completed by the addition of two clamp diodes. The bus voltage is split in two by the connection of equal series connected bus capacitors. The NPC inverter can produce three voltage levels on the output: the DC bus plus voltage, zero voltage and DC bus negative voltage. Therefore the total number of IGBTs is twelve that needs twelve signals controls which can be generated by a PWM controller.

2.4 PWM control of the NPC inverter

PWM is a commonly used technique for controlling inverters. It is based on the comparison of two signals. In this paper a triangular wave with two reference sinusoidal waves (the sinusoidal wave and its opposite) is considered. In addition, a closed loop control is performed using a PID controller for each phase. This controller was chosen with coefficients $K_p = 0.0221$, $K_i = 0.0315$ and $K_d = 0$. The control circuit is sketched in Fig. 5.

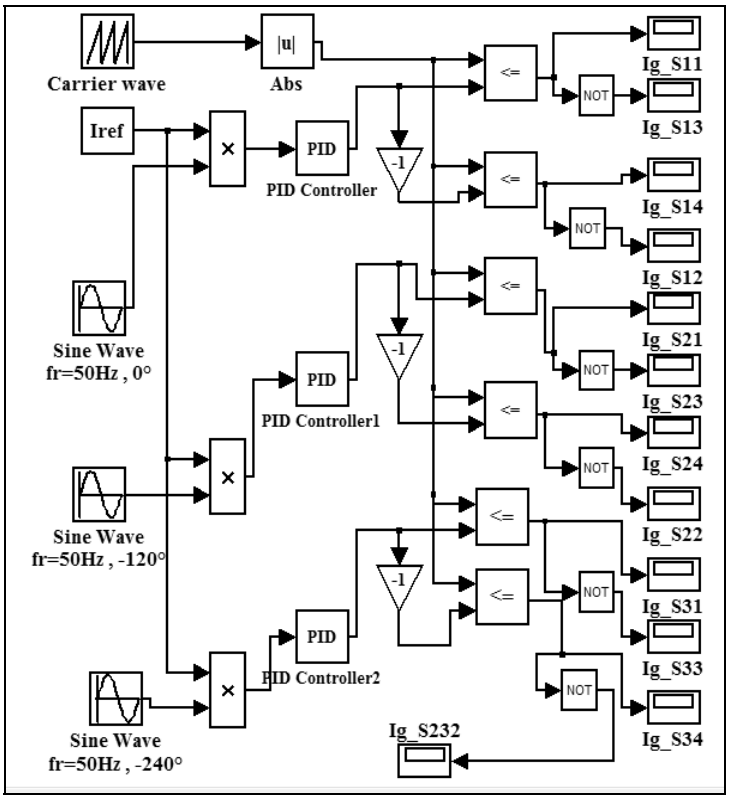

Fig. 5 – *PWM control of the twelve IGBTs.*

3 Simulation of the Global System

The simulation diagram of the overall system is shown in Fig. 6. At the entrance of the diagram, a manual switch selects one of these inputs to pass through the output. The intensity of solar radiation (variable or constant) is chosen. Consequently, the output of the switch is connected to the block diagram of the solar module which in turn feeds a DC/DC converter, controlled by the current I_{ref} generated by an MPPT controller:

$$I_{ref} = I_{MPP} \times N_P , \tag{24}$$

where: N_P is the number of branches in parallel and I_{MPP} the value of current at the maximum power point.

At the output of the DC/DC, an inverter is inserted in the circuit. This is controlled by a strategy based on the PWM which uses a positive triangular signal compared with two reference signals (the sinusoidal signal and its opposite). Outputs of the inverter are connected to the grid and a RL load through an LCL filter. In order to obtain the desired input voltage of the DC/DC converter, 19 modules in series are chosen.

3.1 Simulation results with a constant solarradiation

The scheme of the global grid connected photovoltaic system is given in Fig. 6. As input, the solar radiation of 1000 W/m^2 is considered.

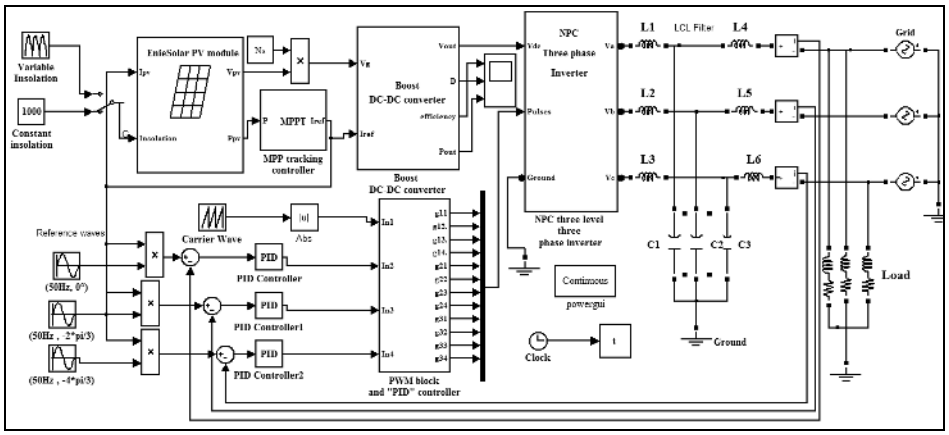

Fig. 6 – *Simulation scheme of global grid connected photovoltaic system.*

3.1.1 Simulation results before the inverter

Areas of low voltage are of two types:

- The low-voltage grid "A" where 50 V < $V_{grid} \leq$ 500 V.
- The low-voltage grid "B" where 500 V < $V_{grid} \leq$ 1000 V.

Simulation results corresponding to the second type are presented.

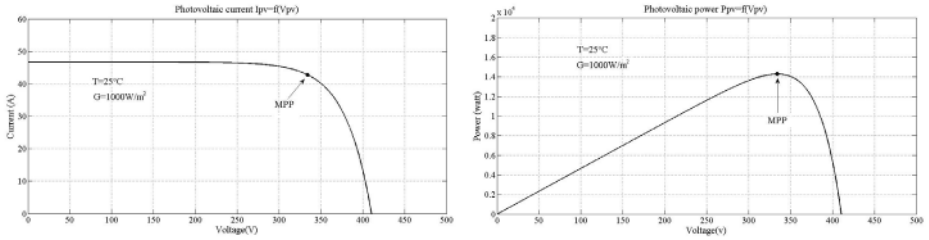

Fig. 7 – *Characteristic of the ENIESOLAR Photovoltaic Generator at the STC conditions.*

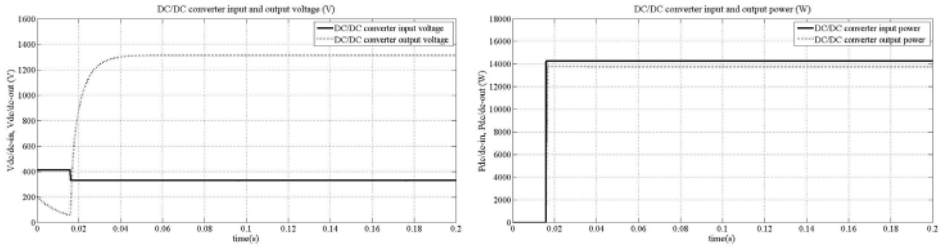

(a) (b)

Fig. 8 – *DC/DC boost converter parameters:* (a) *Input and output voltage;* (b) *Input and output power.*

From Fig. 8a the output voltage is amplified by the DC/DC converter. This input voltage which was equal to: $V_{PV} = N_S \times V_{MPP} = 19 \times 17.3 = 328.7$ V becomes equal to 1314.8 V ((19) gives $D = 0.75$). Input and output powers of the DC/DC converter are presented in Fig. 8b. From both, Fig. 8b and calculation, an efficiency of 0.938 is found.

3.1.2 Simulation results after the inverter

3.1.2.1 Simulation results with grid disconnected for constant solar radiation

The simulation results are presented in Figs. 9, 10 and 11.

At the beginning of the MPPT algorithm, i.e. at $t = 0$, the power P_{PV} is equal zero which explains the operation in open circuit ($V_{PV} = V_{OC} = 410.4$ V). After a sampling time which is considered < 0.01, the voltage V_{PV} drops to the value $V_{MPP} = 328.7$ V.

The inverter output voltage (before the filter) is shown in Figs. 9, 10 and 11. It is a PWM signal where the carrier wave frequency is equal to 3 kHz (which is low) and the same for the currents. At the beginning of the simulation the inverter is powered by the capacitor initially charged. Once the capacitor is discharged, the inverter is powered by the photovoltaic source.

Figs. 12a, 13a and 14a illustrate the current before and after the filter in each phase. A transitional regime is observed which ends a period of 0.02 s there where the current is very large. This can be explained by the fact that the grid sends the current to the system. This leads to use a filter with a coil having a resistor of a few ohms.

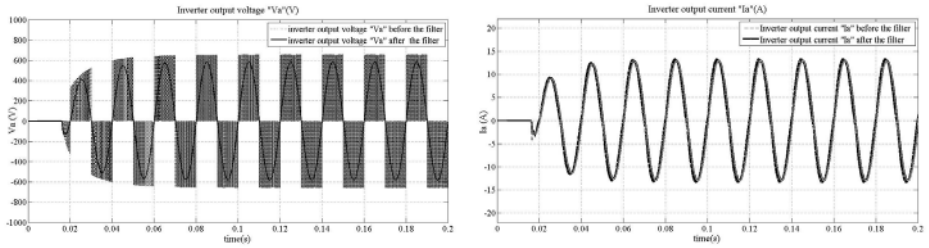

(a) (b)

Fig. 9 – *Inverter output parameters for the phase "a"* (*with grid disconnected*)
(a) *Output voltage "V_a" before and after the filter;*
(b) *Output current "I_a" before and after the filter.*

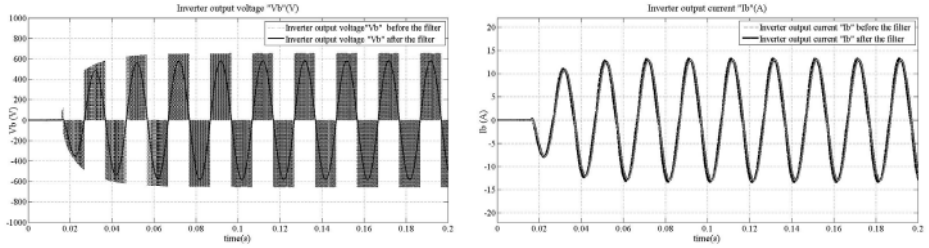

(a) (b)

Fig. 10 – *Inverter output parameters for the phase "b"* (*with grid disconnected*):
(a) *Output voltage "V_b" before and after the filter;*
(b) *Output current "I_b" before and after the filter.*

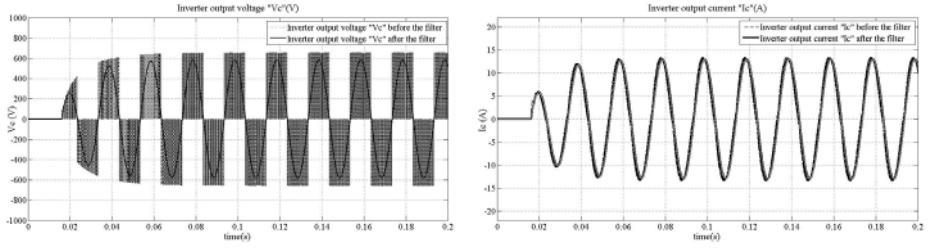

(a) (b)

Fig. 11 – *Inverter output parameters for the phase "c"* (*with grid disconnected*):
(a) *Output voltage "V_c" before and after the filter;*
(b) *Output current "I_c" before and after the filter.*

From $t = 0.025$ s, the system is powered by the photovoltaic source. Therefore the output current of the inverter supplies the load and the remaining current is injected into the grid. Figs. 12b, 13b and 14b show waveforms of various currents.

3.1.2.2 Simulation results with grid connected for constant solar radiation

When the grid is connected, the following simulation results are obtained (see Figs. 12 – 15).

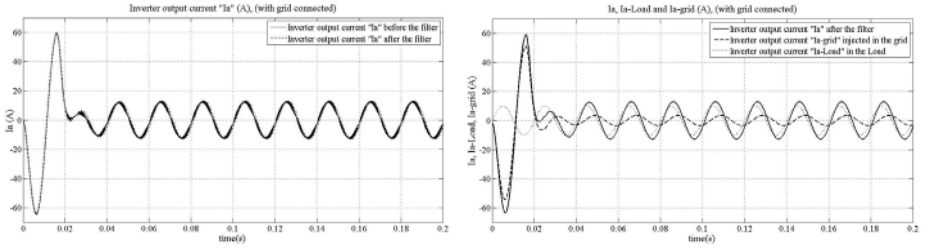

(a) (b)

Fig. 12 – *Inverter output current "I_a"* (*with grid connected*):
(a) *Inverter output current "I_a" before and after the filter;*
(b) *Inverter output currents "I_{af}", $I_{a\text{-}Load}$ and $I_{a\text{-}grid}$.*

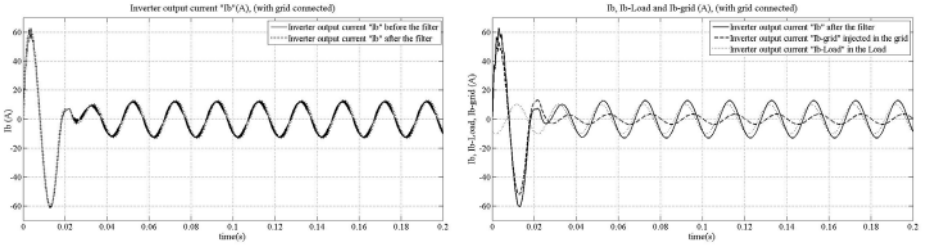

(a) (b)

Fig. 13 – *Inverter output current "I_b"* (*with grid connected*):
(a) *Inverter output current "I_b" before and after the filter;*
(b) *Inverter output currents "I_{bf}", $I_{b\text{-}Load}$ and $I_{b\text{-}grid}$.*

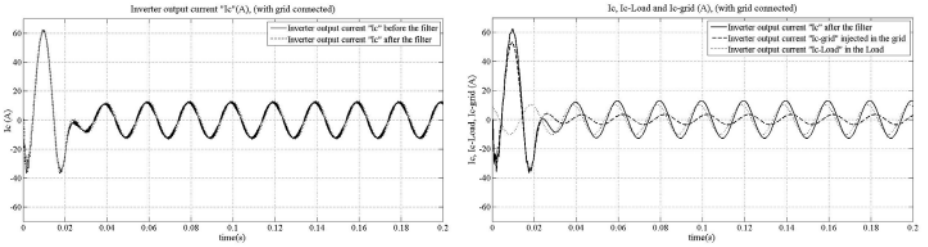

(a) (b)

Fig. 14 – *Inverter output current "I_c"* (*with grid connected*):
(a) *Inverter output current "I_c" before and after the filter;*
(b) *Inverter output currents "I_{cf}", $I_{c\text{-}Load}$ and $I_{c\text{-}grid}$.*

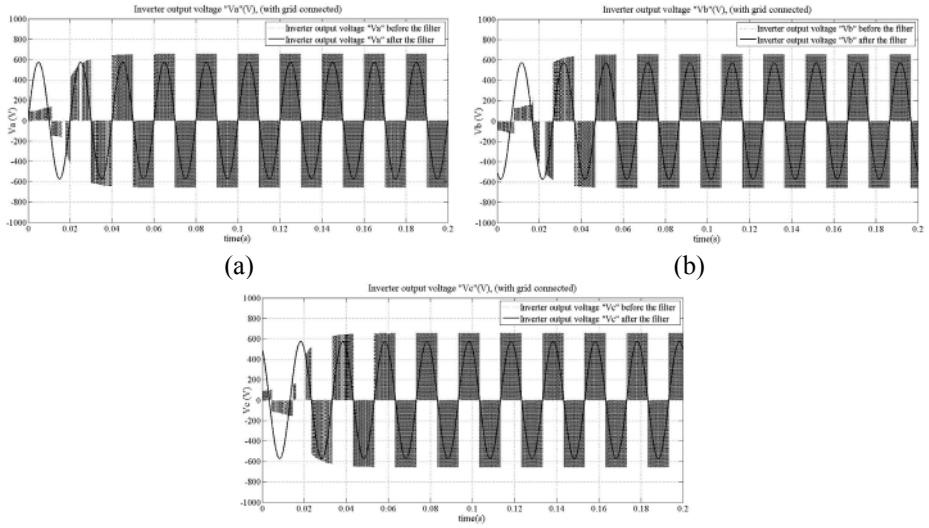

Fig. 15 – *Inverter output voltage* (*with grid connected*): (a) *Voltage "V_a" for phase "a";* (b) *Voltage "V_b" for phase "b";* (c) *Voltage "V_c" for phase "c".*

3.1.2.3 Efficiency of the inverter for constant solar radiation

To calculate the efficiency the average power output of the inverter, given by the following expression, must be determined:

$$P_{out\text{-}inv} = \frac{1}{T}\int_0^T p_{out\text{-}inv}(t)\,\mathrm{d}t = \frac{1}{T}\int_0^T \left[p_a(t) + p_b(t) + p_c(t)\right]\mathrm{d}t\,, \tag{25}$$

where $p_{out\text{-}inv}(t)$ is the sum of the instantaneous powers of the three phases (which are respectively $p_a(t)$, $p_b(t)$ and $p_c(t)$), with

$$p_a(t) = v_a(t)\times i_a(t) = V_{\max}\sin\left(\omega t - \varphi\right) I_{\max}\sin\left(\omega t\right), \tag{26}$$

$$p_b(t) = v_b(t)\times i_b(t) = V_{\max}\sin\left(\omega t - \varphi - \frac{2\pi}{3}\right) I_{\max}\sin\left(\omega t - \frac{2\pi}{3}\right), \tag{27}$$

$$p_c(t) = v_c(t)\times i_c(t) = V_{\max}\sin\left(\omega t - \varphi - \frac{4\pi}{3}\right) I_{\max}\sin\left(\omega t - \frac{4\pi}{3}\right). \tag{28}$$

Substituting these powers by their expressions in equation (25) yields:

$$\begin{aligned} P_{out\text{-}inv} = \frac{1}{T}\int_0^T p_{out\text{-}inv}(t)\,\mathrm{d}t = \frac{1}{T}\int_0^T \Big[& V_{\max}\sin\left(\omega t - \varphi\right) I_{\max}\sin\left(\omega t\right) + \\ & + V_{\max}\sin\left(\omega t - \varphi - \frac{2\pi}{3}\right) I_{\max}\sin\left(\omega t - \frac{2\pi}{3}\right) + \\ & + V_{\max}\sin\left(\omega t - \varphi - \frac{4\pi}{3}\right) I_{\max}\sin\left(\omega t - \frac{4\pi}{3}\right)\Big]\mathrm{d}t, \end{aligned} \tag{29}$$

where $V_{\max} = \sqrt{2}V_{rms}$ and $I_{\max} = \sqrt{2}I_{rms}$, ($V_{rms}$ and I_{rms} are respectively the RMS values of the voltage and the current in each phase, φ is the phase shift between the voltage and the current.

After calculation, the average power output of the inverter becomes:

$$P_{out\text{-}inv} = 3V_{rms}I_{rms}\cos(\varphi). \tag{30}$$

The inverter efficiency is given by:

$$\eta_{DC/AC} = \frac{P_{out\text{-}inv}}{P_{DC/DC}}. \tag{31}$$

The DC/DC converter output power and the average power output of the inverter are presented in Fig. 16.

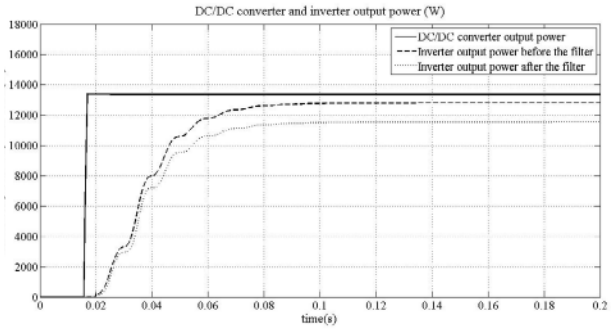

Fig. 16 – *DC/DC converter output , inverter output and filter output powers.*

By using equations (23) and (29), efficiencies of the DC/DC converter and the inverter are presented in Fig. 17.

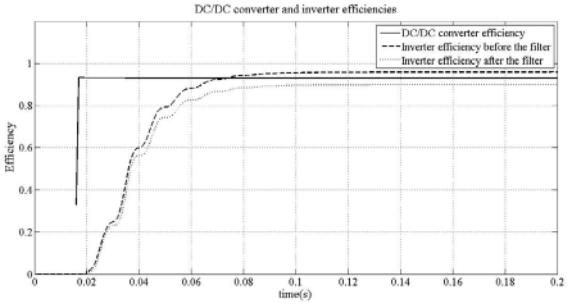

Fig. 17 – *Efficiency of the DC/DC converter and the inverter.*

The filter used in this work is an LCL filter because it is very suitable in the case where the PV system is connected to the grid. As it is shown in Fig. 16, the DC/DC converter output power is 13366.5 W and the inverter output power is 12835 W before the filter but the power after the filter is only 11623.5 W. This

is due to the Joule effect losses in the resistances of the filter coils which are taken equal to 1 Ω each. These losses can be reduced on one hand by decreasing the values of the coils resistances. On the other hand, by using equations (23) and (29) the efficiencies of the DC/DC converter and the inverter are respectively: $\eta_{DC/DC} = 0.938$ and $\eta_{DC/AC} = 0.96$. According to the latest value, the losses in the inverter switches are very low and they can be neglected. These losses represent On-state losses, Off-state losses, Turn-on losses and Turn-off losses and can be calculated from the expressions given in the references [9, 10].

3.2 Simulation Results with a Variable Solar Radiation

Solar radiation is simulated as a curve which starts with low values in the morning and evolves over time to reach a peak value (1000 W/m^2) at noon and then decreases in the evening. The number of hours of sunshine is greater or equal to 9 hours i.e. for weather conditions called Type "A" [11]. In this work, the number of hours is taken equal to 15 hours. Knowing that the period of sinusoidal signal equals to 0.02 s (which is very negligible to 24 hours). So a simulation time of 24 h×3600 = 86400 s divided by 100000 which gives a value of 0.864 s is taken to visualize the behavior of voltages and currents at the inverter output. The simulation time is given to imitate the behavior of a real solar radiation (see Fig. 18).

The simulation results with grid connected are given as follows:

In Fig. 19a, a marked amplification of the converter input voltage is observed. By using (19) the duty cycle of the boost converter D = 0.75 is found. The efficiency of the boost converter η = 0.938 is obtained by using Fig.19b and (23).

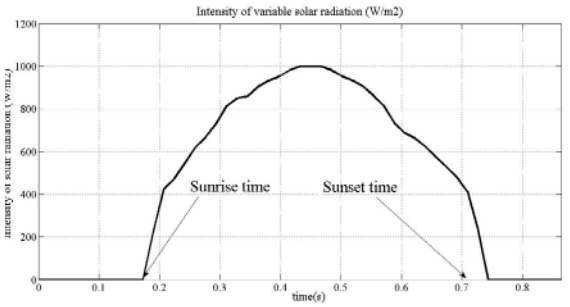

Fig. 18 – *Daily variable solar radiation.*

Figs. 20a, 21a and 22a show the voltages of the three phases before and after the output filter. All these figures are accompanied with an enlargement at the beginning of the simulation (see Figs. 20b, 21b and 22b), where the inverter is fed by the capacitor.

In Fig. 23, one cycle of the voltages is shown where for each phase voltage before the filter has a rectangular shape, with a peak value of 657.4 V that is virtually equal to the DC/DC converter voltage divided by two. The voltage after the filter is a sine wave with a peak value of 575 V. The difference between the two voltage values is due to the voltage drop across the filter.

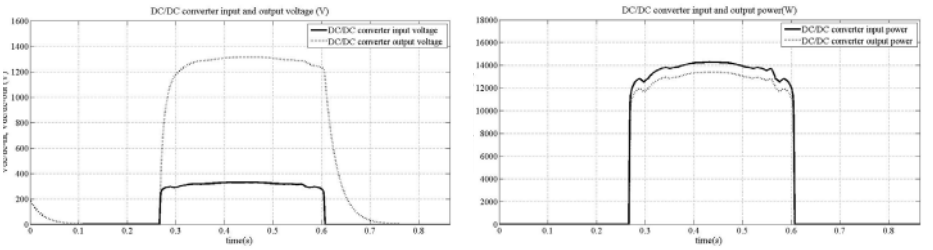

(a) (b)

Fig. 19 – *DC/DC boost converter parameters:*
(a) *Input and output voltage;* (b) *Input and output power.*

3.2.1 Simulation results with grid disconnected for variable solar radiation

Fig. 24 shows the three phase inverter output currents before the filter, they start with low values then they reach their peak values of 13.5 A at noon and finally drop to zero in the absence of radiation. The sinusoidal shape of the output currents of the inverter, sketched on Fig. 25, is very clear. One cycle of currents is shown in Fig. 26.

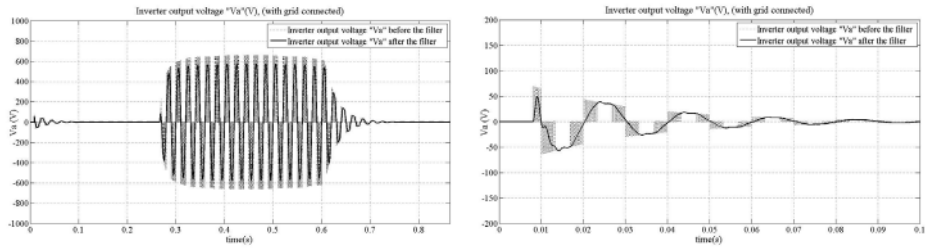

(a) (b)

Fig. 20 – *Inverter output voltage "V_a" before and after the filter* (*with grid disconnected*):
(a) *Voltage "V_a" for the variable solar radiation;*
(b) *Enlargement of the voltage "V_a" at the beginning of simulation.*

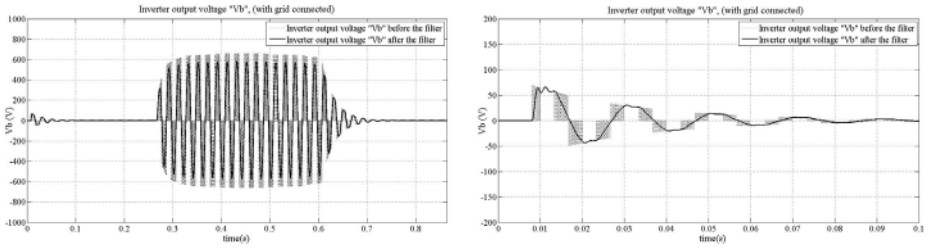

(a) (b)

Fig. 21 – *Inverter output voltage "V_b" before and after the filter* (*with grid disconnected*): (a) *Voltage "V_b" for the variable solar radiation;* (b) *Enlargement of the voltage "V_b" at the beginning of the simulation.*

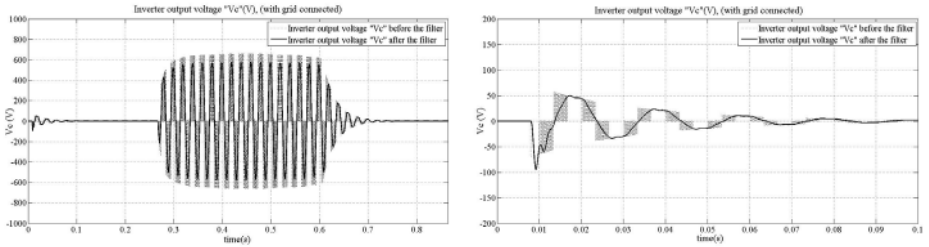

(a) (b)

Fig. 22 – *Inverter output voltage "V_c" before and after the filter* (*with grid disconnected*): (a) *Voltage "V_c" for the variable solar radiation;* (b) *Enlargement of the voltage "V_c" at the beginning of simulation.*

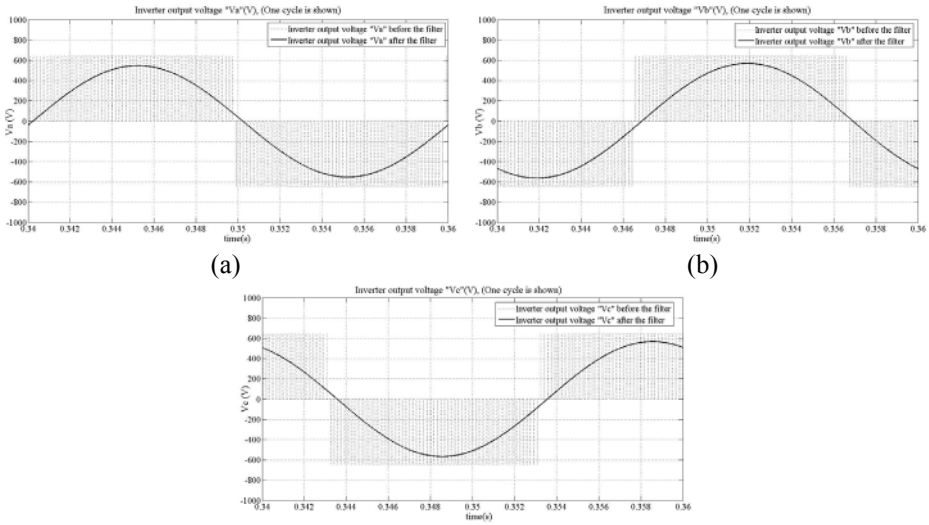

(a) (b)

(c)

Fig. 23 – *Inverter output voltages "V_a", "V_b" and "V_c" before and after the filter* [*one cycle is shown*]: (a) V_a; (b) V_b; (c) V_c.

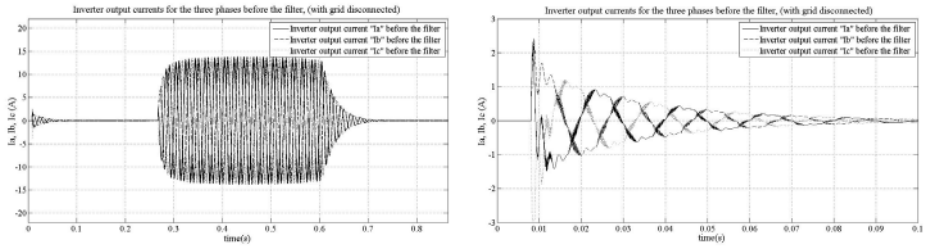

(a) (b)

Fig. 24 – *Inverter output currents before the LC filter* (*with grid disconnected*)
(a) *Currents:"I_a", "I_b" and "I_c" for the variable solar radiation;*
(b) *Enlargement of the currents:"I_a", "I_b" and "I_c" at the beginning of simulation.*

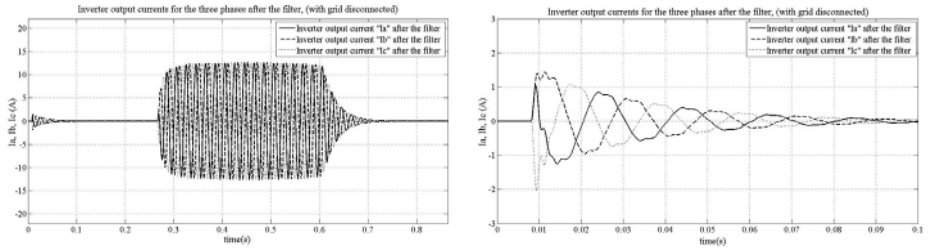

(a) (b)

Fig. 25 – *Inverter output currents after the LC filter* (*With grid disconnected*):
(a) *Currents:"I_a", "I_b" and "I_c" for the variable solar radiation;*
(b) *Enlargement of the currents: "I_a", "I_b" and "I_c" at the beginning of simulation.*

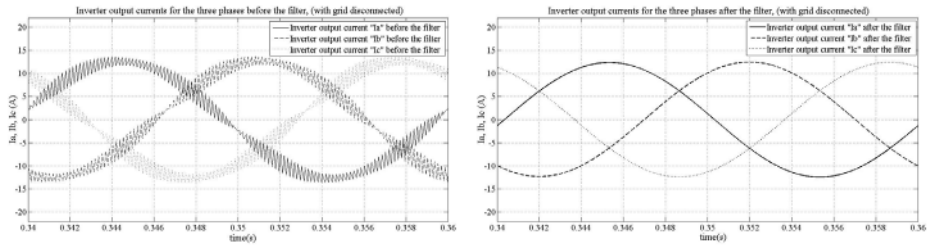

(a) (b)

Fig. 26 – *Inverter output currents "I_a", "I_b" and "I_c"* [*One cycle is shown*]:
(a) *"I_a", "I_b", "I_c" before the filter;* (b) *"I_a", "I_b", "I_c" after the filter.*

3.2.2 Simulation results with grid connected for variable solar radiation

Fig. 27 shows the voltages of three phases, before and after the filter, at the output of the inverter. Before the filter, it is observed that the voltages start with a small value (equal to that of the capacitor divided by 2 (V_{dc}/2 = 200/2 = 100 V)), then they increase more and more up to t = 0.26 s where the photovoltaic source starts to charge the system. The corresponding currents (Fig. 28) start with a

high value (around 65 A) which lasts for a period of 0.02 s (33 minutes in reality) at the value of 13.5 A. Inverter output currents for each phase are presented in Fig. 29, wherein at $t = 0$ a transition period where the current imposed by the grid is clearly equal the sum of the current supplied to the system and that which supplies the load. But when solar radiation reaches a high enough value the photovoltaic system supplies the load and sends the remaining current in the grid, then it tends to zero in the evening because the radiation is low, and the load is fed back via the grid.

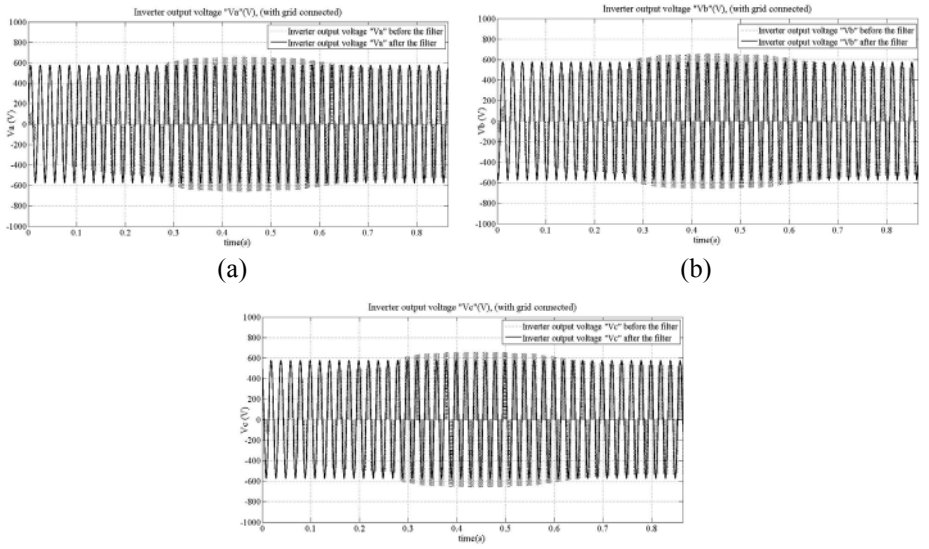

Fig. 27 – Inverter output voltage before and after the filter with grid connected:
(a) Voltage "V_a" for phase "a"; (b) Voltage "V_b" for phase "b";
(c) Voltage "V_c" for phase "c".

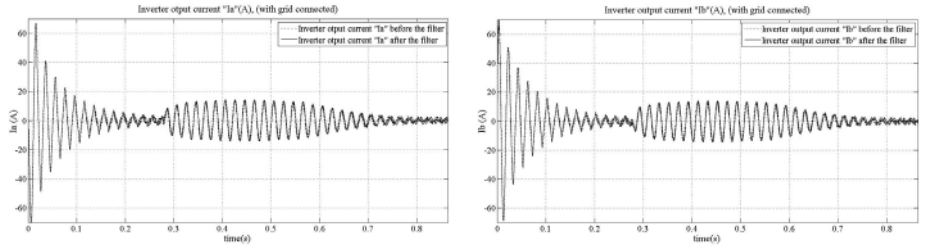

Fig. 28 – *Inverter output current after the filter* (*with grid connected*):
(a) *Inverter output current "I_a" before and after the filter;*
(b) *Inverter output current "I_b" before and after the filter*;

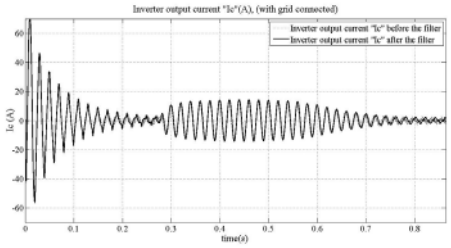

Fig. 28c – *Inverter output current after the filter* (*with grid connected*): *Inverter output current "I_c" before and after the filter.*

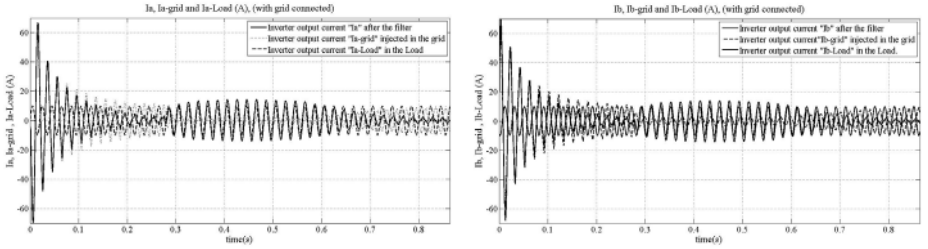

(a) (b)

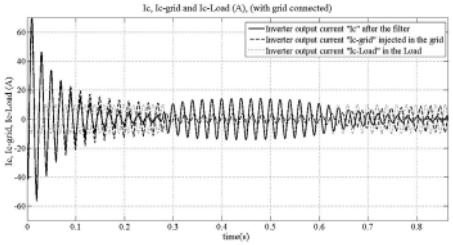

Fig. 29 – *Inverter output current* (*with grid connected*):
(a) *Inverter output currents "I_{af}", $I_{a\text{-}Load}$ and $I_{a\text{-}grid}$;*
(b) *Inverter output currents "I_{bf}", $I_{b\text{-}Load}$ and $I_{b\text{-}grid}$*
(c) *Inverter output currents "I_{cf}", $I_{c\text{-}Load}$ and $I_{c\text{-}grid}$.*

3.2.3 Efficiency of the inverter for variable solar radiation

Fig. 30 illustrates the input and the output power of the inverter (before and after the filter). The output power of the inverter before the filter is almost equal to the input power, giving efficiency equal to 0.96. This shows that the switching and the conduction losses in the switches of the inverter are negligible. Therefore, the power after the filter is significantly lower than the input power, which gives efficiency equals to 0.9. So, it is very clear that the Joule effect losses in the filter are responsible for this decrease.

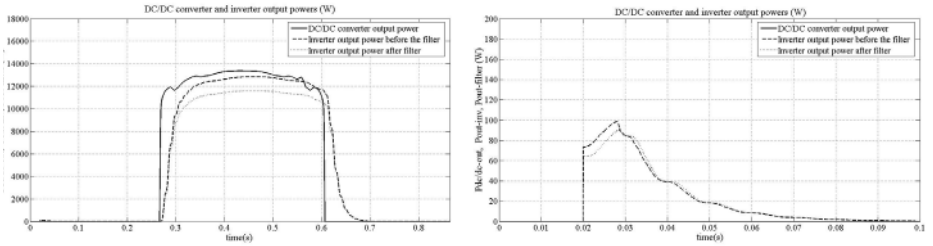

(a) (b)

Fig. 30 – *Inverter input and output power* (*with grid disconnected*):
(a) *Inverter output power throughout the day;*
(b) *Enlargement of the powers at the beginning of simulation.*

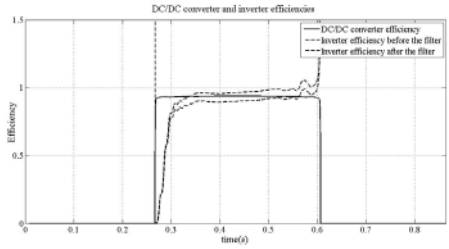

Fig. 31 – *DC/DC converter and inverter efficiencies.*

3.2.4 Fast Fourier Transform (FFT) analysis

The Fast Fourier Transform (FFT) analysis, using the POWERGUI block, yields to the following results:

Table 1

The THD (%) *of the voltage and the current of phase "a" for three values of "f_c".*

Phase "*a*"	THD (%)		
	f_c = 50Hz	f_c = 1000 Hz	f_c = 3000 Hz
I_{anf}	64.49	25.54	16.54
I_{af}	42.45	2.49	0.15
V_{anf}	37.43	58.74	57.71
V_{af}	44.01	4.10	0.18

In the **Table 1**, the Total Harmonic Distortion (THD) is given for phase "*a*" for three switching frequencies. The THD decrease with increasing frequency is observed. The best results are obtained for the frequency f_c = 3 kHz, where: f_c is the carrier wave frequency in PWM control. I_{anf} and V_{anf} are respectively the

unfiltered current and voltage of the phase "*a*", I_{af} and V_{af} are respectively the filtered current and voltage of the phase "*a*". The magnitude of the fundamental harmonic and the THD value are given by Fig. 32.

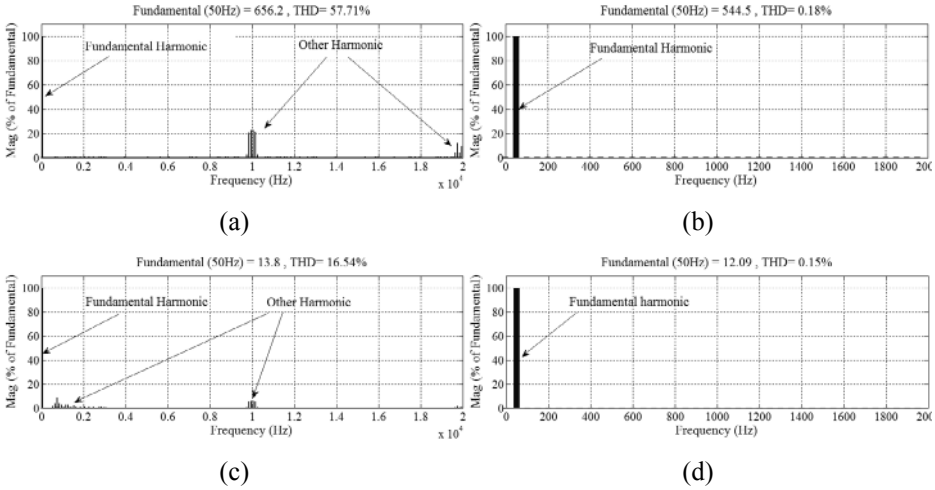

Fig. 32 – *Spectrum of the inverter output voltage and current after the filter for phase "a":*
(a) *Spectrum of the unfiltered inverter output voltage* V_{anf}*;*
(b) *Spectrum of the unfiltered inverter output current* I_{anf}*;*
(c) *Spectrum of the filtered inverter output voltage* V_{af}*;*
(d) *Spectrum of the filtered inverter output voltage* I_{af}*.*

In the case of a constant solar radiation (Fig. 32) it is observed that the response of the DC/DC converter and the inverter is very fast, i.e. at t less than 0.01 s all parameters (voltages and currents), appear at inputs and outputs of the two converters. Therfore, in the case of variable solar radiation, the response of the DC/DC boost converter and the inverter is slow. All parameters (voltage and current) at the inputs and outputs of the converters appear at $t = 0.26$ s, the response is zero at low values of solar radiation, which means that the DC/DC boost converter and the inverter operate from $t = 0.26$ s to $t = 0.60$ s, i.e. from 7:25am to 04:40pm. The operating real time is 10 hours and 45 minutes.

4 Conclusion

In this paper the simulation study in Matlab/Simulink of a grid connected photovoltaic three-phase NPC inverter with DC/DC boost converter has been presented. The control of this inverter is based on a PWM strategy which uses a carrier wave with low frequency equal to 3 kHz and two reference signals. A MPPT controller (with P&O algorithm) is used to generate current control of the DC/DC boost converter. The inverter is simulated for two patterns of solar

radiation, one is constant and the other is variable. The obtained results are satisfactory despite the low value of the frequency of the carrier wave PWM control strategy. The only drawback is the presence of Joule effect losses in the filter which reduce slightly the efficiency of the inverter. On the other hand, the use of an open-loop control has an effect on the amplitude of the sinusoidal voltage at the output of the inverter. But, this problem is overcome with the use of a current closed-loop control based on the addition of PID controllers.

When the PV system is connected to the grid it is necessary to use an LCL filter with coil resistance of a few ohms. Also a multi-level inverter can be used where the output voltage is with a number of levels greater than three.

The THD obtained for the voltages and the currents are very low (< 1.0%) which are good results. The advantage of the inverter is, on the one hand, the series connection of IGBTs will increase the voltage at its input without fear of overvoltage. On the other hand, other IGBTs can be added to the inverter in order to be connecting to the medium voltage grid.

5 Parameters of ENIESOLAR module

"ENIESOLAR" is a solar module manufactured by the National Company Electronic Industries in Algeria, which characteristics are given as follow:

Parameter	value
Maximal power	75 W, ± 10%
Short circuit current I_{SC}	4.67 A
Open circuit voltage V_{OC}	21.6 V
MPP voltage V_{MPP}	17.30 V
MPP current I_{MPP}	4.34 A
minimum value of the fuse in series	10 A
number of cells in series	36
number of cells in parallel	1

5 References

[1] M. Calais, V. Agelidis: Multilevel Converters for Single-phase Grid Connected Photovoltaic Systems –An Overview, International Symposium on Industrial Electronics, Pretoria, South Africa, 07 – 10 July 1998, Vol. 1, pp. 224 – 229.

[2] L.M. Tolbert, F.Z. Peng, T. Habetler: Multilevel Converters for Large Electric Drives, IEEE Transactions on Industry Applications, Vol. 35, No. 1, Jan./Feb. 1999, pp. 36 – 44.

[3] J. Rodriguez, J.S. Lai, F.Z. Peng: Multilevel Inverters: Survey of Topologies, Controls and Applications, IEEE Transactions on Industry Applications, Vol. 49, No. 4, Aug. 2002, pp. 724 – 738.

[4] E. Pouresmaeil , O. Gomis-Bellmunt, D. Montesinos-Miracle, J. Bergas-Janea: Multilevel Converters Control for Renewable Energy Integration to the Power Grid, Energy, Vol. 36, No. 2, Feb. 2011, pp. 950 – 963.

[5] R.H. Baker, L.H. Bannister: Electric Power Converter, U.S. Patent 3867643, Feb. 1975.

[6] F.M. Gonzalez-Longatt: Model of Photovoltaic Module in Matlab™, 2nd Latin American Congress of Students of Electrical, Electronics and Computer Engineering, Puerto La Cruz, Venezuela, 03 – 07 April 2006.

[7] C. Nelson, J. Williams: Boost Converter Operation, LT1070 Manual Design, Application Note 19, June 1986.

[8] J.S. Kumari, C.S. Babu, A.K. Babu: Design and Analysis of P&O and IP&O MPPT Techniques for Photovoltaic System, International Journal of Modern Engineering Research, Vol. 2, N o. 4, July /Aug. 2012, pp. 2174 – 2180.

[9] U. Drofenik, J.W. Kolar: A General Scheme for Calculating Switching- and Conduction-losses of Power Semiconductors in Numerical Circuit Simulations of Power Electronic Systems, International Power Electronics Conference, Niigata, Japan, 04 – 08 April 2005.

[10] F. Schafmeister, C. Rytz, J.W. Kolar: Analytical Calculation of the Conduction and Switching Losses of the Conventional Matrix Converter and the (Very) Sparse Matrix Converter, Applied Power Electronics Conference and Exposition, Austin, TX, USA, 06 – 10 March 2005, Vol. 2, pp. 875 – 881.

[11] G.N. Tiwari, S. Dubey: Fundamentals of Photovoltaic Modules and their Applications, RSC Publishing, Cambridge, UK, 2010.